Journal of Medicinal Chemistry

pubs.acs.org/jmc

Article

Effect of Flexibility, Lipophilicity, and the Location of Polar Residues on the Passive Membrane Permeability of a Series of Cyclic Decapeptides

Shuzhe Wang, Gerhard König, Hans-Jörg Roth, Marianne Fouché, Stephane Rodde, and Sereina Riniker*

Cite This: *J. Med. Chem.* 2021, 64, 12761−12773

Read Online

ACCESS | Metrics & More | Article Recommendations | Supporting Information

ABSTRACT: Cyclic peptides have received increasing attention over the recent years as potential therapeutics for "undruggable" targets. One major obstacle is, however, their often relatively poor bioavailability. Here, we investigate the structure−permeability relationship of 24 cyclic decapeptides that share the same backbone N-methylation pattern but differ in their side chains. The peptides cover a large range of values for passive membrane permeability as well as lipophilicity and solubility. To rationalize the observed differences in permeability, we extracted for each peptide the population of the membrane-permeable conformation in water from extensive explicit-solvent molecular dynamics simulations and used this as a metric for conformational rigidity or "prefolding." The insights from the simulations together with lipophilicity measurements highlight the intricate interplay between polarity/lipophilicity and flexibility/rigidity and the possible compensating effects on permeability. The findings allow us to better understand the structure−permeability relationship of cyclic peptides and extract general guiding principles.

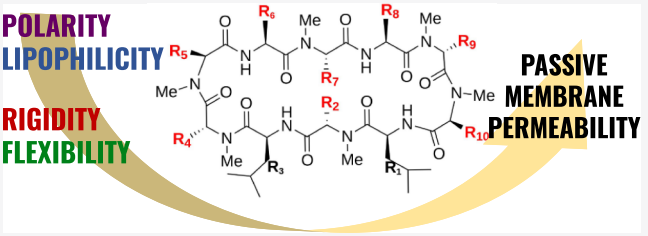

INTRODUCTION

A large portion of currently known disease targets is considered "undruggable" by small molecules that comply with the rule of five (Ro5)[1] for bioavailable drugs.[2] Moreover, the amount of undruggable targets is growing rapidly due to the continuous discovery of new targets, many of which are protein−protein interactions (PPIs).[3] Therefore, the focus has moved to molecules beyond the Ro5 (bRo5) space as potential therapeutics for these difficult targets.[4,5] Within this category, peptides excel in their ability to modulate protein surfaces and PPI interfaces that have large, flat, or groove-shaped binding sites.[6−8] Furthermore, their peptidic nature also leads to fewer toxicity concerns. Cyclization of peptides confines their flexibility,[9] which was generally found to be beneficial for the binding affinity, selectivity within families of related targets, and proteolytic stability.[10,11] Some cyclic peptides have already been turned into marketed drugs and many more are entering clinical trials.[12] Despite these advancements, the success stories so far are mostly based on natural products, indicating that the rational design of cyclic peptide drugs with favorable properties is not trivial. In particular, achieving good membrane permeability and oral bioavailability remains challenging and requires further improvements in our understanding of the structure−permeability relationship of cyclic peptides.[11,13]

It has been hypothesized that the "chameleonic" nature of cyclic peptides, that is, their ability to respond to different dielectric conditions by adapting the conformation, is a key for good passive membrane permeability.[14−17] Cyclic peptides are thought to interconvert between a so-called *closed* conformation in an apolar environment (like the membrane interior) in which the polar groups of the molecule are shielded from the surroundings through intramolecular hydrogen bonds (H-bonds), also called "self-solvation,"[18,19] and open conformations in water where polar groups can form H-bonds to the solvent molecules. The possibility to adopt such a closed conformation is a necessary (but not always sufficient) condition for permeability.[20] To gain insights into the conformational behavior of cyclic peptides and to potentially quantify it, different computational methods have been used in combination with experimental techniques.

Many studies have focused on relatively simple metrics to predict the permeability of cyclic peptides, such as the number of intramolecular H-bonds,[21] partition coefficients,[22] or 3D polar surface area (3D PSA)[23] of the closed, membrane-permeable conformation(s). Recent examples where 3D PSA was found to be an effective indicator for permeability include

Received: April 29, 2021
Published: August 18, 2021

a study by Le Roux et al.[24] with 47 semipeptidic macrocycles (tetramers with an alkyl linker) and one by Poongavanam et al.[25] for a set of 70 diverse macrocyclic molecules. In the latter work, a strong correlation between permeability and 3D PSA was found for one of the stereo- and regioisomeric series of the set, which was relatively rigid. However, no 3D model could outperform the simpler and faster binary classification model based on the 2D topological fingerprint on the whole set. Kamenik et al.[26] performed MD simulations on six small peptidomimetics and used 3D PSA to cluster the trajectories, from which free energies were calculated to correlate with permeability. However, not all studies found good correlations between the 3D PSA and permeability. In the work by Ono et al.[27] on eight hexapeptides, ensemble 3D PSA from solvents of varied polarities showed poor correlation with permeability, while the average solvent-accessible surface area (SASA) from cyclohexane simulation was a good indicator. Cipcigan et al.[28] also found 3D PSA to be ineffective in comparison to other metrics such as molecular globularity for their series of six pentapeptides. Similarly, we could not detect correlations between ensemble 3D PSA and permeability in our study of four semipeptidic tetramers.[29] Instead of focusing on the PSA, Hoang et al.[30] calculated the largest connected hydrophobic surface area for 16 molecules categorized into six series of varied sizes (including mainly hexa-, heptapeptides, and two undeca-peptides). Within each series of 2−4 peptides, the hydrophobic surface area correlated well with permeability. Other recent studies investigated the use of single-point energy calculations of NMR structures[31] or multivariate regression models based on experimental observables and simulation data[32] to predict permeability.

Most of the recent studies discussed above have focused on relatively small peptides with limited ring flexibility. However, the available conformational space of cyclic peptides increases dramatically with the ring size, which leads to sampling problems with conventional computational methods. To address this issue, approaches based on MD simulations are among the most promising. For example, Lokey and co-workers used multicanonical MD simulations[34] in a recent study[33] to assess the conformational flexibility of cyclic decapeptides (CDPs) in different solvents. In our group, we developed an approach based on extensive parallel MD simulations starting from diverse conformations in polar and apolar solvents. The resulting trajectories are used to build core-set Markov models (CSMMs)[35−37] that inform us about the metastable conformational states of a peptide in different environments. This workflow has been applied to investigate the conformational dynamics of cyclosporines,[38,39] CDPs,[40] and cyclic octadepsipeptides.[41]

In our previous study on CDPs,[40] we investigated a series of six compounds with the same backbone scaffold and N-methylation pattern but different residues at two positions in the ring. While the closed conformation was found to be the major conformation for all peptides in chloroform and no correlation between the 3D PSA and membrane permeability could be observed, the differences in permeability between the peptides emerged in the conformational behavior in water. We observed that the population of the closed conformational state in the CSMM in water correlated well with the experimental permeability. In this study, we extend our work on the CDPs from Fouché et al.[42,43] and systematically vary the residue positioning and side chain composition of the scaffold to yield a larger set of 24 decapeptides. The backbone scaffold of the CDPs with six N-methylations is still the same throughout the series. As shown in Figure 1A, the side chains of residues 2 and

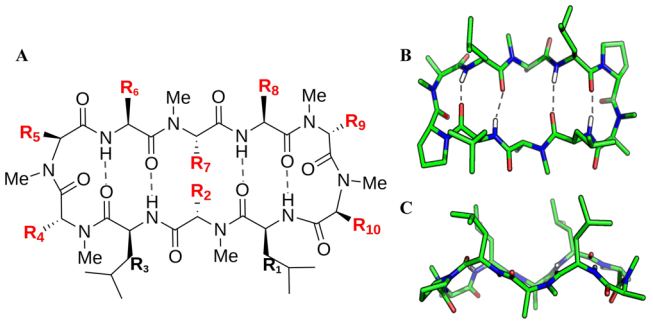

Figure 1. (A) Schematic illustration of the CDP scaffold with modifications at residues 2, 4, 5, 6, 7, 8, 9, and 10 (highlighted in red). Residues 1 and 3 are leucines in all peptides. Residues 5 and 10 are D-amino acids to enable the correct β-hairpin conformation.[43] (B) Top view of CDP **2** as an example of the *closed* conformation. (C) Side view of the same 3D conformation.

4−10 are modified, while residues 1 and 3 are leucines in all peptides. The closed conformation as observed in crystal structures and NMR solution structures in chloroform is depicted for CDP **2** as an example in Figure 1B,C. Residues 1, 2, 3 and 6, 7, 8 form the two β-strands, while the two β-turns consist of residues 4, 5 and 9, 10. In this conformation, the backbone is oriented such that all unmethylated amide nitrogen atoms point into the ring and form four typical transannular H-bonds. If the closed conformation is populated in a polar and apolar environment, it can be viewed as a congruent conformation.[38] Based on the extended set of 24 decapeptides, we study the relationship between the conformational preferences and membrane permeability. In addition, we extract mechanistic insights from the formation of the metastable conformational states from the MD trajectories.

RESULTS AND DISCUSSIONS

Based on the findings for CDPs **1**−**6** reported in ref 40, we wanted to investigate the following two main effects with side chain modifications: (1) *polarity*: variation of the number and location of polar residues (mainly threonine) and (2) *rigidification*: variation of the number of proline residues in the β-turns. The resulting set of 24 peptides together with their experimental and computed properties is summarized in Table 1. The population of the closed conformation (identified by the four transannular H-bonds) is obtained from postprocessing MD trajectories of the peptides in water with the CSMM[35−37] framework. In this study, we adapted the previous CSMM protocol slightly to include the more accurate hierarchical density clustering algorithm[44] to identify the microstates. The resulting populations of the closed conformation in water for CDPs **1**−**6** remain largely the same, with some minor changes. The most pronounced difference is for CDP **3**, where the hierarchical clustering gives a cleaner metastable state for the closed conformation, leading to a reduction in the reported population (Table 1). Nevertheless, the observed correlation between the corrected populations and parallel artificial membrane permeation (PAMPA) values still holds for these six peptides (Figure S1 in Supporting Information). It is also important to note that, although the slowest timescale of transition obtained from the CSMM may not have fully converged for all peptides, the relative

https://doi.org/10.1021/acs.jmedchem.1c00775
J. Med. Chem. 2021, 64, 12761−12773

Table 1. Summary of the 24 CDPs Studied with Modifications at Residues 2, 4, 5, 6, 7, 8, 9, and 10: Population (in %, with Uncertainty Estimate from Bootstrapping) of the Closed Conformation in the MD Simulations in Water and Experimentally Measured Passive Membrane Permeability (PAMPA log P_e, More Negative Means Less Permeable), Lipophilicity (log *D* in Decadiene/Water at pH = 7.4, log *D* in Octanol/Water at pH = 7.4, and Calculated clog *P*[45]) as Well as Aqueous Solubility (in mM) and Molecular Weight (MW).[a]

CDP	R_2	R_4	R_5	R_6	R_7	R_8	R_9	R_{10}	popul. [%]	PAMPA log P_e	log *D* d/w	log *D* o/w	clog *P*	solub. [mM]	MW [Da]
1	Me-Ala	D-Pro	Me-Phe	Leu	Me-Ala	Leu	D-Pro	Me-Thr	61 ± 2	−4.3	3.7	5.7	10.8	0.065	1093
2	Me-Ala	D-Pro	Me-Ala	Leu	Me-Ala	Leu	D-Pro	Me-Ala	67 ± 3	−4.6	2.5	4.7	10.1	0.794	987
3	Me-Ala	D-Pro	Me-Thr	Leu	Me-Ala	Leu	D-Pro	Me-Thr	35 ± 1	−5.1	1.2	3.8	8.8	0.884	1047
4	Me-Ala	D-Pro	Me-Phe	Leu	Me-Ala	Leu	D-Pro	Me-Phe	45 ± 4	−5.3	>3.5	>5.7	12.9	0.004	1139
5	Me-Ala	Me-Gly	L-Pro	Leu	Me-Ala	Leu	Me-Gly	L-Pro	15 ± 1	−6.7	0.3		9.0	>1.000	959
6	Me-Ala	Me-D-Ala	Me-Phe	Leu	Me-Ala	Leu	Me-D-Ala	Me-Phe	6 ± 1	−5.9	5.1		13.2	0.004	1115
7	Me-Ala	D-Pro	Me-Ala	Leu	Me-Thr	Leu	D-Pro	Me-Ala	16 ± 1	−5.8	1.7		9.4	0.763	1017
8	Me-Thr	D-Pro	Me-Ala	Leu	Me-Thr	Leu	D-Pro	Me-Ala	5 ± 3	<−6.5	1.0		8.8	0.445	1047
9	Me-Ala	D-Pro	Me-Ala	Leu	Me-Thr	Leu	D-Pro	Me-Thr	9 ± 1	<−6.5	1.2		8.8	>1.000	1047
10	Me-Thr	D-Pro	Me-Thr	Leu	Me-Thr	Leu	D-Pro	Me-Ala	6 ± 0.4	<−6.5	0.4		8.1	0.827	1077
11	Me-Thr	D-Pro	Me-Thr	Leu	Me-Thr	Leu	D-Pro	Me-Thr	12 ± 1	<−6.5	-0.8		7.5	>1.000	1107
12	Me-Ala	D-Pro	Me-Phe	Leu	Me-Thr	Leu	D-Pro	Me-Phe	64 ± 2	−5.0	5.0	5.7	12.2	0.004	1169
13	Me-Ala	D-Pro	Me-Phe	Leu	Me-Ala	Thr	D-Pro	Me-Phe	24 ± 1	−3.9	3.6	5.1	10.8	0.020	1127
14	Me-Ala	D-Pro	Me-Phe	Thr	Me-Ala	Leu	D-Pro	Me-Phe	31 ± 2	−4.7	4.0	5.4	10.8	0.015	1127
15	Me-Ala	D-Pro	Me-Ala	Leu	Me-Ala	Thr	D-Pro	Me-Ala	34 ± 1	−6.5	0.1	2.6	8.0	>1.000	975
16	Me-Ala	D-Pro	Me-Ala	Thr	Me-Ala	Leu	D-Pro	Me-Ala	42 ± 0.3	−5.9	0.4	2.7	8.0	>1.000	975
17	Me-Ala	Me-D-Ala	Me-Val	Leu	Me-Ala	Leu	Me-D-Ala	Me-Val	25 ± 1	−4.8	3.8	5.2	12.2	0.560	1019
18	Me-Ala	D-Pro	Me-Val	Leu	Me-Ala	Leu	Me-D-Ala	Me-Val	33 ± 2	−4.3	4.0	5.2	12.1	0.220	1031
19	Me-Ala	D-Pro	Me-Val	Leu	Me-Ala	Leu	D-Pro	Me-Val	40 ± 1	−4.4	3.8	5.1	11.9	0.057	1043
20	Me-Ala	D-Pro	L-Pro	Leu	Me-Ala	Leu	Me-D-Ala	Me-Val	29 ± 2	−4.6	3.1	5.1	11.0	0.092	1015
21	Me-Ala	D-Pro	L-Pro	Leu	Me-Ala	Leu	D-Pro	L-Pro	33 ± 3	−6.6	1.6	4.3	9.7	0.220	1011
22	Me-Ala	Me-D-Ala	Me-Ala	Leu	Me-Ala	Leu	Me-D-Ala	Me-Ala	16 ± 2	−4.0	2.7	4.6	10.4	0.477	963
23	Me-Ala	D-Hyp	Me-Ala	Leu	Me-Ala	Leu	D-Pro	Me-Ala	59 ± 2	<−6.9	0.2	4.1	9.1	0.910	1003
24	Me-Ala	D-Hyp	Me-Phe	Leu	Me-Ala	Leu	D-Hyp	Me-Thr	65 ± 2	<−6.9	−0.6	4.7	8.9	0.320	1125

[a]Residues 1 and 3 are leucines in all peptides. Note that log *D* is equivalent to log *P* in this study as all 24 CDPs are neutral at pH = 7.4.

https://doi.org/10.1021/acs.jmedchem.1c00775
J. Med. Chem. 2021, 64, 12761−12773

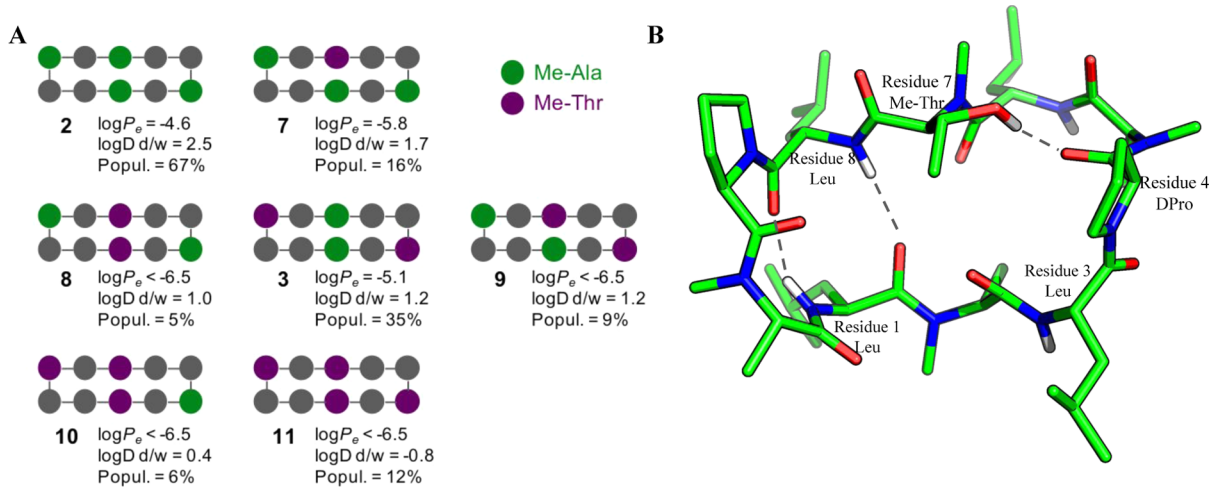

Figure 2. (A) Schematic illustration of the composition of CDPs **2**, **3**, and **7**−**11**. Methylated alanine residues are shown in green and methylated threonine residues are shown in purple. Gray residues are either leucines or D-prolines (at position 4/9). (B) Snapshot of CDP **7** in which the hydroxy group of the threonine at position 7 in the strand disrupts the formation of two of the four transannular H-bonds.

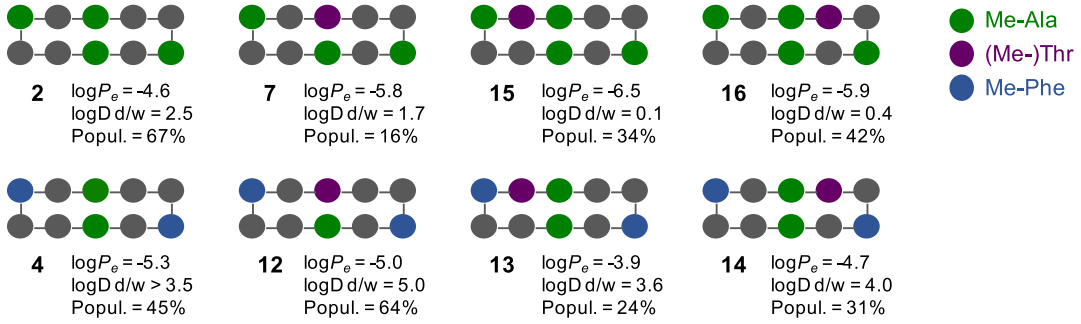

Figure 3. Schematic illustration of the composition of CDPs **2**, **4**, **7**, and **12**−**16**. Methylated alanine residues are shown in green, methylated threonine residues are shown in purple, and methylated phenylalanine residues are shown in blue. Gray residues are either leucines or D-prolines (at position 4/9).

comparison of the differences in the steady-state populations of the metastable sets is possible (see the discussion in ref 40).

Variation of Polar Residues: Number and Location. Motivated by the good permeability of CDP **3** with two threonine residues, we wanted to investigate how many polar side chains can be tolerated and what effect the location within the scaffold has. The base is CDP **2** with D-prolines at positions 4 and 9, leucines at positions 1, 3, 6, and 8, and no threonines. CDPs **3** and **7**−**11** have a varied number and location of the threonine residues (in the strand vs in the turn), as illustrated in Figure 2A. Replacing alanine with threonine increases the polarity of the peptide but enables potential directed interactions with a target binding site. The calculations for CDPs **7**−**11** were performed prospectively, that is, the peptides were synthesized and measured experimentally in parallel.

Compared to CDP **3** with two threonines at the turns, the population of the closed conformation in water and likewise the PAMPA permeability drop dramatically for CDP **7** with a single threonine at position 2 in the strand (Table 1). The addition of more threonine residues in CDPs **8**−**11** worsens the results further. The metastable states of the CSMMs are too coarse to identify the potential cause for this behavior. Therefore, we extracted the most abundant H-bond patterns for each peptide in this series, which involve any of the threonine side chains (summary in Table S1 in Supporting Information). In all cases, we observe an interaction between the hydroxy group of the threonine at position 7 and the backbone oxygen of residues at the turn. This disrupts the pattern of the four transannular H-bonds such that only two of the four can be formed (left side of the peptide shown in Figure 2B). Such a strong interaction of the side chain with the backbone is not observed when the threonine residues sit at the turns due to steric hindrance (the D-prolines rigidify the β-turns), suggesting that it may be the cause for the decreased population of the closed conformation. These findings indicate that not only the number of polar residues is important but also the location in the scaffold.

Location of Threonines in the Strand. Next, we investigated the influence of the location of threonine within the strand (i.e., positions 7, 8, and 9) for two scaffolds (Figure 3). In CDPs **7**, **15**, and **16**, the base scaffold is again CDP **2** with methylated alanine and D-proline in the β-turns. For all three peptides, the addition of a polar residue in the strand leads to a decrease in the population of the closed conformation, most pronounced for CDP **7** with the threonine at position 7 (Table 1). As discussed above, threonine at this position can form H-bonds with the backbone of the turn residues, preventing the formation of the four transannular H-bond patterns of the closed conformation. For CDPs **15** and **16**, on the other hand, only local H-bonds are observed (Table S1 in Supporting Information). As can be seen in the side view of the peptide in the closed conformation as shown in Figure

https://doi.org/10.1021/acs.jmedchem.1c00775
J. Med. Chem. 2021, 64, 12761−12773

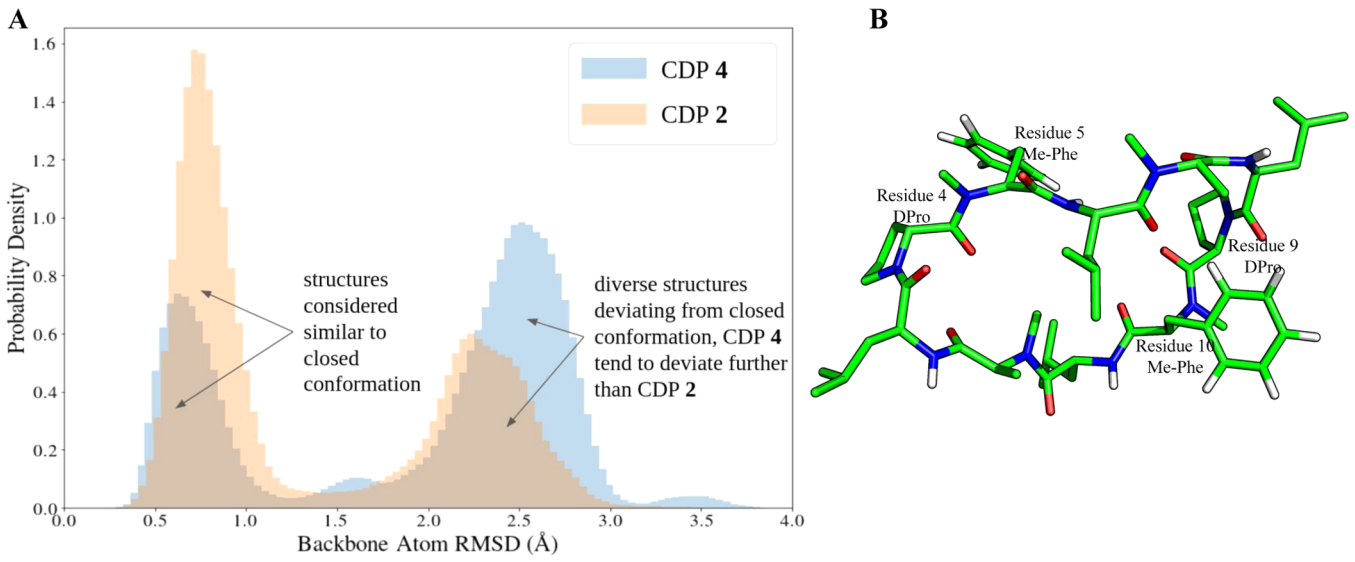

Figure 4. (A) Distribution of the backbone atom-positional root-mean-square deviation (RMSD) with respect to the closed conformation of CDP **2** and **4**. (B) Snapshot of CDP **4** showing how a register shift moves the phenylalanine residues from being at the turns in the closed conformation into the strand regions.

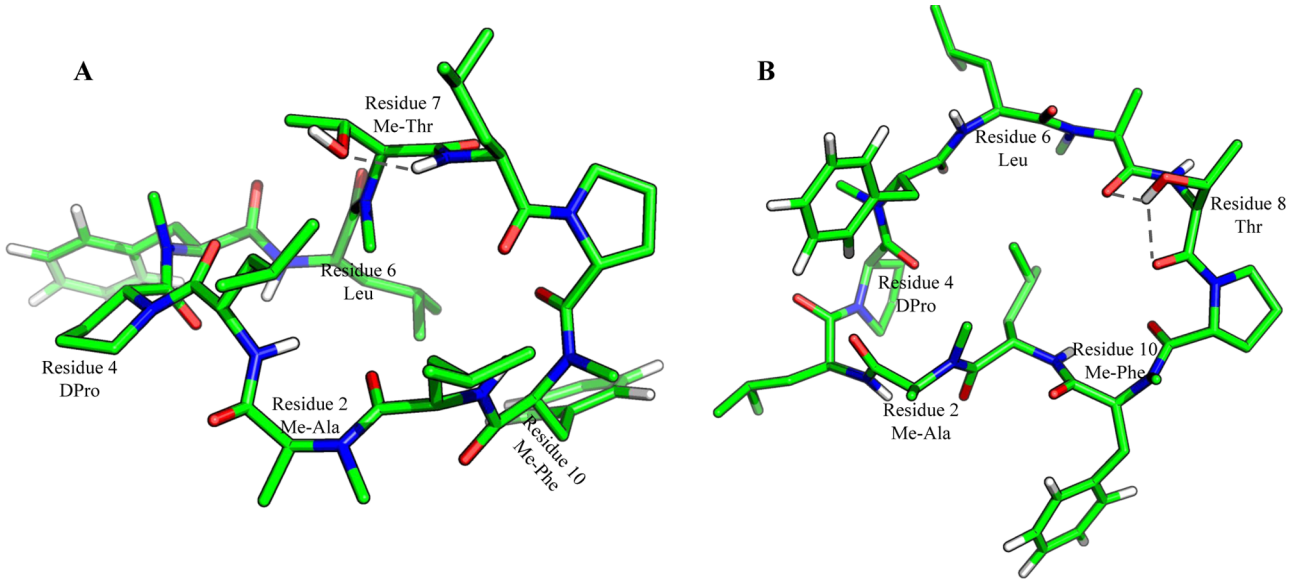

Figure 5. (A) Snapshot of CDP **12** showing how the side chain threonine at position 7 can act as the H-bond acceptor to the backbone unmethylated amide nitrogen (position 8) to prevent it from pointing away from the macrocyclic ring. (B) Snapshot of CDP **13** showing how the side chain threonine at position 8 can act as the H-bond donor to two amide oxygen atoms that stabilizes a pose where the backbone unmethylated amide nitrogen (position 8) points away from the macrocyclic ring.

1C, the side chains at positions 6 and 8 point in the opposite direction than the side chain at position 7. On the side of residues 6 and 8, the methylated amide nitrogen at the turn cannot form H-bonds with the hydroxy group of threonine. Thus, the population of the closed conformation is decreased to a lesser extent than for CDP **7**. The PAMPA permeability, however, is low for all three peptides. As a leucine residue is replaced by threonine in CDPs **15** and **16**, these peptides have comparatively high polarity as measured by log *D* decadiene/water (Table 1). This indicates that above a certain threshold, even the closed conformation becomes too polar for good permeability. This is in line with studies where the number of intramolecular H-bonds differs between the low-permittivity conformation of macrocycles.[16,22,23,27,29,31]

CDPs **12**−**14** have the same variation of threonine at positions 7, 8, and 9, with CDP **4** as the base scaffold. Compared to the previous series, the methylated alanines in the turns are replaced by more bulky phenylalanine residues. The phenylalanines increase the lipophilicity dramatically as reflected in the log *D* decadiene/water measurements (Table 1). Interestingly, the experimental properties of the second series exhibit very different trends compared to the first series. The introduction of threonine does not lead to a decrease in lipophilicity, and instead, even a slight increase is observed. Similarly, the permeability is not reduced but remains comparable or even increases substantially in the case of CDP **13** (giving the highest PAMPA log P_e value of the 24 peptides). Furthermore, while the permeability of CDP **4** is

https://doi.org/10.1021/acs.jmedchem.1c00775
J. Med. Chem. 2021, 64, 12761−12773

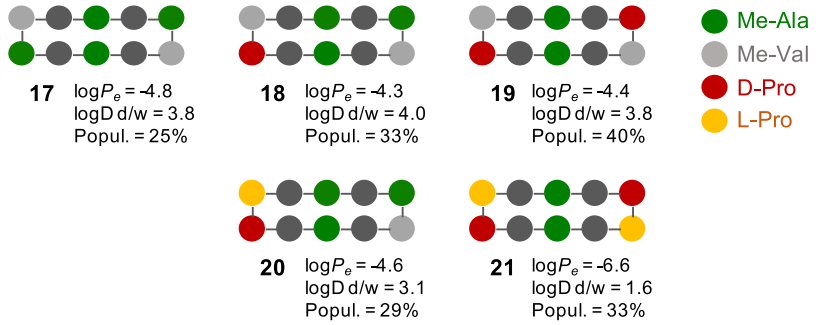

Figure 6. Schematic illustration of the composition of CPDs **17**−**21**. Methylated alanine residues are shown in green, methylated valine residues are shown in light gray, D-proline residues are shown in red, and L-proline residues are shown in orange. Dark gray residues are leucines.

lower than that of CDP **2**, the opposite is the case for CDPs **12**−**14** and their counterparts in the first series. These findings indicate that the threonine and phenylalanine residues can have compensating effects.

When replacing the alanines in the turns of CDP **2** with phenylalanines in the case of CDP **4**, the permeability is reduced (from log P_e = −4.6 to −5.3) and so is the population of the closed conformation in water (from 67 to 45%). In addition, the open conformations of CDP **4** tend to deviate more from the closed conformation compared to CDP **2** due to a "register shift" (i.e., the phenylalanine residues are no longer at the turns), as shown in Figure 4.

The populations of the closed conformation in water for CDPs **12**−**14** do not follow the trend in the experimental permeability and also not the trend of the counterparts in the first series (Table 1). We again considered the most frequently occurring H-bond patterns for each peptide to rationalize the effect of the threonine location in the strand (Table S1 in Supporting Information). In the conformations with a register shift as observed with the phenylalanines, the unmethylated amide nitrogen in the strand (the backbone of residue 8) is rotated such that it points outward of the macrocycle and can no longer form a transannular H-bond. In the case of CDPs **13** and **14**, such a conformation is further stabilized by a H-bond between the threonine and the backbone nitrogen (Figure 5B), which hinders the reorientation of the amide. This leads to a reduction in the population of the closed conformation. For CDP **12**, the opposite effect is observed. In this case, the hydroxy group of threonine forms a H-bond with the neighboring unmethylated amide nitrogen at position 8, which prevents the backbone from rotating (Figure 5A). Thus, the distortive effects of the phenylalanines and the threonine at position 7 partially compensate each other, resulting in a high population of the closed conformation. We also observe this behavior with CDP **7** but far less frequently. Similarly, the interaction of threonine with the backbone oxygen turn found with CDP **7** is not observed with CDP **12**, possibly due to the more rigid backbone of the phenylalanines.

In the previous and this series, the total amount of polarity is hardly changed; merely the location of the polar residue is different which can lead to large log *D* differences. This suggests that lipophilicity is not only affected by residue composition but also residue interactions. The computed closed population supports the finding and analysis of the simulation trajectories can give indications to the reasoning.

Taken together, the experimental and computational results indicate that the effective lipophilicity (or polarity) of these cyclic peptides is not just determined by the amino acid composition (i.e., how many polar groups are present) but also influenced by the location of the residues and the intramolecular interactions affecting the conformational ensemble. Furthermore, the findings suggest that the population of the closed conformation in water becomes less important for very lipophilic peptides.

Rigidification: Prolines in the *β*-Turns. A major conclusion from the study of CDPs **1**−**6** mentioned in ref 40 was that the D-prolines at positions 4 and 9 rigidify the *β*-turns, resulting in higher populations of the closed conformation in water. In the following, we investigated this effect systematically with CDPs **17**−**21** (Figure 6). The base scaffold is CDP **17** without any prolines. We decided to place valines at position 5/10 in the turns to have a less flexible residue but not phenylalanine due to the solubility issues (all peptides with two phenylalanines have a very low solubility in water). CDP **18** has one D-proline at position 4, CDPs **19** and **20** have two prolines either at both turns or at the same turn, and CDP **21** has four prolines (Figure 6). The calculations for this series were again performed prospectively, that is, the peptides were synthesized and tested in parallel.

Due to the valines at the turns, the lipophilicity of CDP **17** is high (log *D* decadiene/water = 3.8) such that the permeability is already good (log P_e = −4.8) at a comparatively low population of the closed conformation in water (25%). When introducing one D-proline at the turn in CDP **18**, we observe a small increase in the population of the closed conformation water (to 33%) and likewise in the PAMPA permeability (to log P_e = −4.3). Introducing a second proline (either symmetrically as in CDP **19** or in the same turn as in CDP **20**) does not significantly alter the population of the closed conformation, the permeability, or lipophilicity. Having two prolines at opposite turns instead of one turn appears to be slightly better, that is, 40% population and log P_e = −4.4 for CDP **19** versus 30% population and log P_e = −4.6 for CDP **20**. An exception is CDP **21** with four prolines. While the population of the closed conformation (as identified with four transannular H-bonds) remains similar to the other CDPs in this series, the experimental permeability drops dramatically (log P_e = −6.6) and likewise the lipophilicity (log *D* decadiene/water = 1.6). In the simulations, we find that the closed conformation is twisted to some degree compared to the other peptides but the four transannular H-bonds are preserved. The drop in lipophilicity is, however, an indication that the polar groups are no longer properly shielded in the case of CDP **21**, possibly due to the twisting caused by too many prolines in the cycle.

https://doi.org/10.1021/acs.jmedchem.1c00775
J. Med. Chem. 2021, 64, 12761−12773

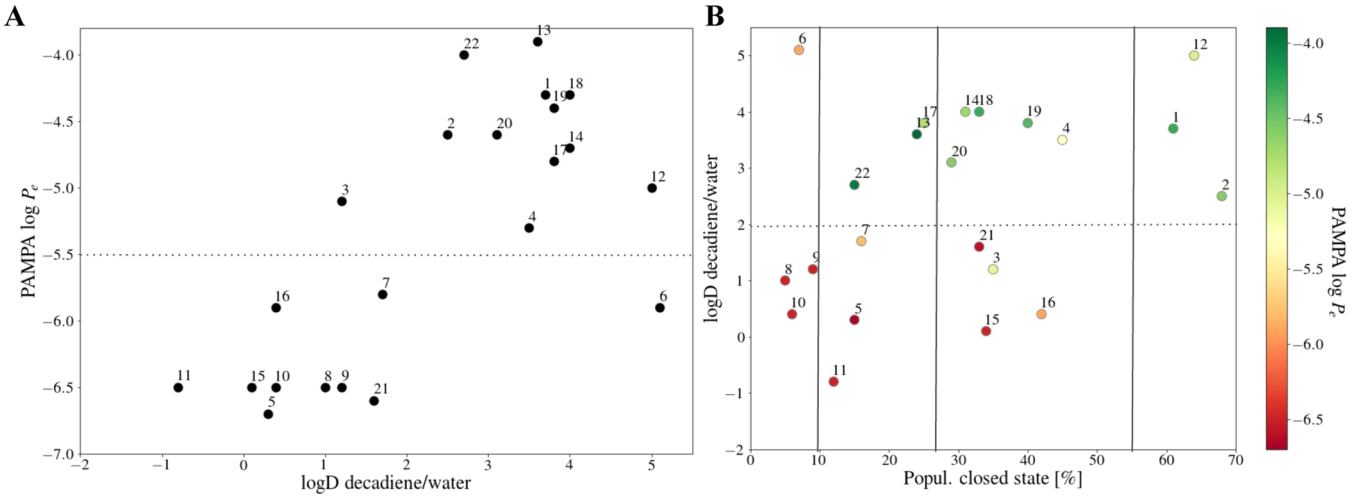

Figure 7. (A) PAMPA permeability log P_e vs lipophilicity (log D decadiene/water) for CDPs **1**−**22** (Table 1). (B) Log D decadiene/water (d/w) versus the population of the closed conformation in water (in %), where the color scale denotes the PAMPA permeability log P_e.

Another exceptional case is presented by CDP **22**, which also has no proline residues like CDP **17** and methylated alanines instead of valines in the turns. The lipophilicity is, therefore, reduced compared to CDP **17** but still relatively high (log D decadiene/water = 2.7). Without any rigidifying prolines and the flexible alanines in the turns, the population of the closed population in water is lowered (16%) as can be expected. Nevertheless, CDP **22** has a PAMPA log P_e of −4.0 (among the highest in the set). It is not clear from the simulations what causes this high permeability.

Hydroxyprolines in the Turns. The results discussed above suggest that D-prolines in the turns are generally beneficial for permeability and that threonine residues can be best tolerated in the turns. Therefore, we wanted to investigate if the effect of both proline and threonine could be combined by placing one or two D-hydroxyprolines at positions 4 and 9. As base scaffolds, we used CDPs **1** and **2**. The calculations were again carried out prospectively. While experimentally, all four variants were tested, simulations were performed only for two of them. Thus, we report in Table 1 only the results of CDP **23**, which is a variant of CDP **2** with one hydroxyproline (i.e., one polar group in the peptide), and of CDP **24**, which is a variant of CDP **1** with two hydroxyprolines (i.e., three polar groups in the peptide). As hydroxyprolines have the same rigidifying effect of the β-turns as prolines, the populations of the closed conformation in water remain close to that of CDPs **1** and **2**. However, experimentally, these two peptides were found to be polar (log D decadiene/water = 0.2 and −0.6) and nonpermeable (log P_e < −6.3). The experimental results for the other two variants are very similar (data not shown). In this case, the mandatory requirement that all polar groups can be shielded in the apolar phase is no longer given. As the hydroxy groups of the hydroxyprolines cannot engage in transient H-bonds with the backbone due to steric hindrance, some polar groups remain exposed even in the closed conformation.

Comparison Across the Set. The ability of a cyclic peptide to adopt a type of closed conformation where all polar groups are shielded from the apolar environment is a mandatory (but not always sufficient) condition for good permeability.[16,20,22,23,27,31] As this condition is not fulfilled by CDPs **23** and **24** with the hydroxyproline residues, we exclude these two peptides from the following comparison.

Permeability Versus Lipophilicity. It has already been observed early on that permeability coefficients of small nonelectrolytes correlate well with oil/water partition coefficients (i.e., Overton's rule from 1899).[46−50] While this relationship can be nearly linear over stretches of the lipophilicity scale, it is essentially bilinear or parabolic over the entire range.[47,48,51] If a molecule is highly polar, it will not be able to cross the apolar membrane core. In the other extreme of highly apolar molecules, factors such as membrane sequestration and decreasing aqueous solubility become an issue, decreasing the observed apparent permeability. The maximum permeability is obtained at intermediate (in general relatively high) lipophilicity values.

Lokey and co-workers observed this parabolic relationship between permeability (PAMPA log P_e) and lipophilicity (log D decadiene/water or calculated Alog P) for a large set of cyclic hexapeptides[22,52] (e.g., Figure 1D in ref 22) and more recently for two different libraries of CDPs,[33] which were derived from the same backbone scaffold reported in ref 43 as used in our study. The two decapeptide libraries differ in the location of peptoid residues (turn vs strand) and involve mainly apolar side chain modifications. The log D decadiene/water range is, therefore, smaller than for our set of 24 peptides. Interestingly, the peak of the parabolic relationship between log P_e and log D decadiene/water was shifted between the two libraries depending on the flexibility of the backbone scaffold, that is, the more flexible library peaks at higher lipophilicity values (Figure 2a in ref 33).

The expected parabolic relationship is also seen for our smaller set of decapeptides (Figure 7A, even though only CDPs **6** and **12** mark the "too lipophilic" region). For our series, the peak of the parabola is shifted to higher lipophilicity values (log D decadiene/water ≈ 3.5) compared to the libraries reported in ref 33. While there is a clear relationship between permeability and lipophilicity with a window of favorable lipophilicity, log D decadiene/water is not a good metric for the quantitative prediction of log P_e by itself as the permeability range for a given log D decadiene/water value can be large. Examples in our set are CDP **6** versus CDP **12** (log D decadiene/water = 5.1 and 5.0 vs log P_e = −5.9 and −5.0) or

https://doi.org/10.1021/acs.jmedchem.1c00775
J. Med. Chem. 2021, 64, 12761−12773

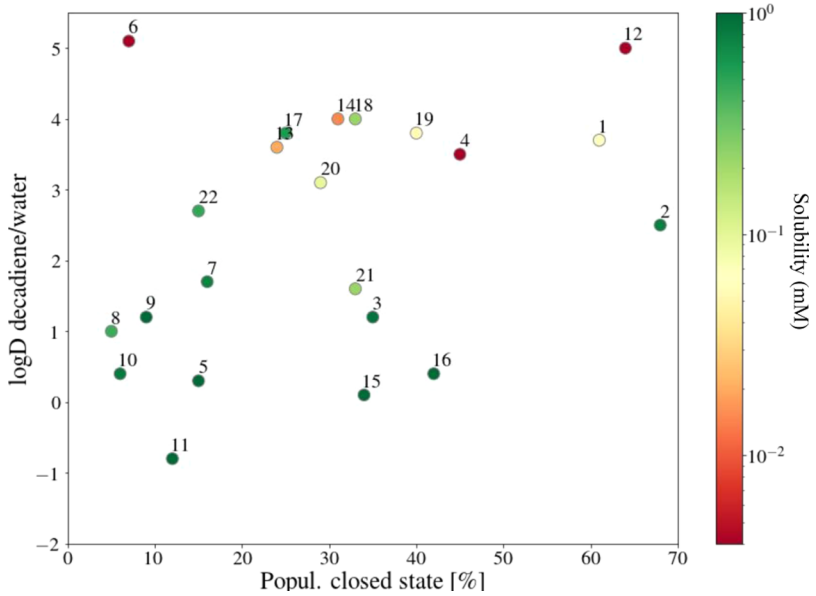

Figure 8. Log *D* decadiene/water (d/w) of CDPs **1**−**22** vs the population of the closed conformation (in %), where the color scale denotes aqueous solubility (in mM on a logarithmic scale).

CDP **9** versus CDP **3** (log *D* decadiene/water = 1.2 and 1.2 vs log P_e = −6.5 and −5.1). Similar broad ranges can also be seen in refs 22 and 33.

Measure of Rigidity/Flexibility. A common model for the permeation process[53] involves two steps (in the case of neutral molecules): (1) conformational locking into the membrane-permeable conformation (i.e., closed conformation for cyclic peptides) and (2) transfer between the polar and apolar phases. Each step is associated with a free energy barrier, and the overall likelihood of the permeation process is an interplay between the heights of both barriers. High lipophilicity will influence the free energy of transfer, making it more favorable for the peptide to partition into the membrane. Locking the peptide in the closed conformation where all polar groups can be shielded from the apolar environment presents a free energy barrier, which can be reduced if the closed conformation is already populated in the polar phase. Rigidity is, therefore, not favorable for permeability per se, rather rigidity in the optimal membrane-permeable conformation is. The more flexible the peptide, the higher is the free energy penalty for locking the conformation.

The kinetic models used in this study offer a fine-grained interpretation of the conformational behavior and flexibility of the peptides. The population of the closed conformation in water can be used as a measure for rigidity, as there are many open conformations possible but only one closed conformation. This is not necessarily reflected in the number of metastable sets in the kinetic models because these show the slowest processes in the system, while the interconversions among open conformations are often relatively fast. It can, however, be seen in the "intracluster" RMSD of the backbone ring (rRMSD), which is generally higher for open conformational states compared to the closed conformational state (see Figures S28−S51 in Supporting Information). This observation suggests that for the presented series of CDPs, a low population of the closed conformation correlates with a higher flexibility of the peptide. When plotting permeability against the population of the closed conformation in water for our set of peptides (Figure S1 in Supporting Information), we see that there is no correlation applicable to the entire set. However, when we plot log *D* decadiene/water against the population of the closed conformation in water and color the points by PAMPA permeability (Figure 7B), we can distinguish different ranges with specific behavior (horizontal lines).

Although our set of 24 peptides is relatively small and more data points will be needed to draw quantitative conclusions, we can extract some trends from Figure 7B. Highly flexible peptides (population of the closed conformation in water < 10%) are poorly permeable, apparently regardless of their lipophilicity. At the other extreme, relatively rigid peptides with a high population of the closed conformation (>55%) tend to have good membrane permeability. The intermediate region can be divided further into two subregions, although this boundary is less defined. When peptides are moderately flexible (approx. 10−28%), permeability shows a strong dependence on lipophilicity. With the increasing population of the closed conformation (approx. 28−55%), lipophilicity becomes less dominant and decent permeability can be achieved even for relatively polar peptides (exemplified by CDP **3**). This indicates that increasing polarity (i.e., higher free energy penalty for the transfer into the apolar phase) can be (partially) compensated by increasing rigidity or "prefolding" of the membrane-permeable conformation (i.e., lower free energy cost for conformational locking). On the other side, higher flexibility can be (partially) compensated by increasing lipophilicity. These observations are in line with the results from the study by Lokey and co-workers with their two libraries of CDPs, where the more flexible library showed a permeability peak at higher lipophilicity values than the more rigid library.[33] In other words, the more flexible peptides required higher lipophilicity to reach the same permeability value as the more rigid peptides.

The experimentally determined log *D* decadiene/water shows for this series of cyclic peptides with a common backbone scaffold good correlation with the calculated (octanol/water) clog *P*[45] (Figure S2 in Supporting Information). Note that this correlation is to some degree coincidental as the correlation with the experimental log *D* octanol/water is

https://doi.org/10.1021/acs.jmedchem.1c00775
J. Med. Chem. 2021, 64, 12761−12773

worse, although this would be the corresponding solvent mixture (Figure S3 in Supporting Information). Nevertheless, the finding suggests that the in silico combination of clog *P* computation with the flexibility analysis based on CSMMs may offer a framework to estimate the passive membrane permeability within a series of cyclic peptides.

Solubility Perspective. For oral administration, it is desirable that a cyclic peptide is not only permeable but also soluble. While relatively high lipophilicity is beneficial for permeability, it is the opposite for solubility. Figure 8 shows a similar plot as Figure 7 but with points colored by solubility. Most peptides in our set with good permeability are poorly soluble. Notable exceptions are CDPs **2**, **17**, and **22** with a log *D* decadiene/water > 2 and an aqueous solubility of 0.79, 0.56, and 0.48 mM, respectively. However, these peptides contain only side chains without polar groups and thus offer fewer possibilities for directional interactions with the binding site of a potential target.

CDP **3** is overall the most interesting variant, as it strikes a compromise between the presence of polar residues (two threonines in the β-turns), which offer the possibility for selective interactions with a potential protein target, moderate flexibility, decent permeability (log P_e = −5.1), and good solubility (0.88 mM). Moderate flexibility is important for the chameleonic nature, with a closed conformation when inside the membrane and the population of more open states in water that can form H-bonds with residues of a target binding site.

CONCLUSIONS

Using CSMMs based on extensive MD simulations, we conducted systematic studies on 24 CDPs, which share the same backbone scaffold but modifications of the side chains. The steady-state population of the closed conformational state in the CSMM in water was used as an indicator for the flexibility/rigidity of the peptides. Our results show that not only the composition of the CDPs (number of proline or threonine residues) can have a large effect on their properties but also the location of specific residues in the scaffold. Especially for polar residues, subtle structural changes can result in large differences in the conformational behavior and ultimately permeability. While it is important that polar side chains can form intramolecular H-bonds in an apolar environment to be shielded (see the examples with hydroxyproline residues), the formation of intramolecular H-bonds with the backbone may also disturb the adoption of the closed conformation (see examples with threonine residues in the β-strands). A careful choice of the location of polar residues within the scaffold is therefore crucial.

High flexibility in water or high polarity (i.e., high free energy cost to enter the membrane) is detrimental to permeability. However, flexibility can be compensated by higher lipophilicity (up to a limit), and some degree of polarity can be tolerated when the membrane-permeable conformation is sufficiently populated in water ("prefolding"). High lipophilicity is, however, often accompanied by poor aqueous solubility. The most interesting cases are therefore CDPs such as **2** and **3** with both medium to good permeability and solubility. In particular, CDP **3** strikes a compromise between moderate rigidity and the presence of two polar residues (at the preferred location in the β-turns), which offer the opportunity for selective interactions with a potential protein target.

For the design of novel cyclic peptides, we would extract the following general principles from our combined findings: (i) choice of a backbone scaffold and an N-methylation pattern that facilitates the adoption of a closed-type conformation in an apolar environment where all unmethylated backbone amides are involved in intramolecular H-bonds, (ii) partial rigidification of the closed conformation through the introduction of turn-stabilizing residues, (iii) careful placement of polar residues (ideally guided by the analysis of the conformational preferences with computational methods), and (iv) counterbalance of polar residues with apolar residues to reach the favorable lipophilicity window.

METHODS

Experimental Measurements. The synthesis of the CDPs has been described in detail in ref 43. Purity assessment was performed by analytical liquid chromatography−mass spectrometry (LC−MS) and LC−UV (220−400 nm DAD) HPLC. The purity of all compounds is >95%

PAMPA Permeability. PAMPA[54] was used as a primary screen to predict gastrointestinal permeability. The assay was carried out in 96-well plates by measuring the ability of the compound to diffuse from a donor to an acceptor plate separated by a 9−10 μm hexadecane liquid layer coated on a polycarbonate filter plate. To minimize solubility issues, compounds were loaded at 5 μm in the donor compartment and the assay buffer contained 5% DMSO. The permeability was derived from the compound concentration measured by LC−MS/MS in the acceptor compartment after a 4 h incubation time.

Log *D* Decadiene/Water. The 1,9-decadiene/water distribution coefficient at pH = 7.4 (log *D* d/w) was determined using the shake-flask equilibrium method. All solvents used for HPLC were of UHPLC-MS grade. 1,9-Decadiene (Sigma-Aldrich, 118303) and PBS (PBS tablets prepared from P4417—Sigma-Aldrich and Milli-Q water) were used. Glass vials (2 mL) with rubber/poly-(tetrafluoroethylene) septa were used for the partitioning test. Rotator PTR-35 (Grant-bio) was used for overnight shaking of the vials. An Eppendorf 5804 centrifuge was used for the phase separation. The quantification was performed using a Vanquish chromatographic system coupled to a high-resolution mass spectrometry (HRMS) instrument, Exactive Plus Orbitrap, both from Thermo Scientific.

The samples were first dissolved in 1,9-decadiene at a target concentration of 1 mM. One vial was used for each phase concentration determination. Milli-Q water was added such that the phase ratio *K* between the two phases was 10 (where $K = V_{water}/V_{1,9\text{-decadiene}}$). Duplicate vials were agitated on a rotator for 20 h at 75 rpm. Subsequently, the vials were centrifuged for 15 min at 3600 rpm by positioning one vial with the cap on top and the other was turned upside down. The upside-down position allows for the sampling of the aqueous phase by using a syringe without the need to pass through the organic phase, thus avoiding any risk of contamination. An adequate dilution in methanol was made for the two phases (×2 and ×200 for the aqueous phase, ×2000 and ×20,000 for the 1,9-decadiene phase), and the samples were quantified by LC−HRMS using a six-point calibration curve.

HPLC conditions: Zorbax SB-Aq 30 × 2.1 mm (1.8 μm) column, oven temperature = 50 °C, mobile phase: *A* = 100% water UHPLC grade + 0.08% formic acid, *B* = 100% acetonitrile + 0.08% formic acid, flow rate = 0.5 μL/min, gradient: starting at 95% *A* up to 95% *B* in 0.5 min and maintained constant during 1 min, before restoring initial conditions within 0.1 min. V_{inj} = 5 μL, and HRMS acquisition mode: full scan 190−1800 m/z and resolution = 35,000.

Log *D* Octanol/Water. The 1-octanol/water distribution coefficient at pH = 7.4 (log *D* oct/w) was determined using the shake-flask equilibrium method. Prior to starting the experiment, the two phases were presaturated, that is, "water-saturated octanol" and "octanol-saturated water" were used. The samples were first dissolved in 1-octanol at a target concentration of 1 mM. One vial was used for

https://doi.org/10.1021/acs.jmedchem.1c00775
J. Med. Chem. 2021, 64, 12761−12773

each phase concentration determination, and the phase ratio K between the two phases was 10.0 (where $K = V_{water}/V_{octanol}$). The duplicate vials were agitated on a rotator for 20 h at 75 rpm. Subsequently, the vials were centrifuged for 15 min at 3600 rpm by positioning one vial with the cap on top and another vial was turned upside down. The upside-down position allows for the sampling of water by using a syringe without the need to pass through the octanol phase and avoids any risk of contamination of the aqueous phase. An adequate dilution was made for the two phases (×2 for the aqueous phase and ×2000 for the octanol phase), and the samples were quantified by LC−HRMS using a six-point calibration curve (Vanquish chromatographic system coupled to Exactive Plus Orbitrap, Thermo Scientific). The column used was Zorbax_SB_AQ 30 × 2.1 mm 1.8 μm, and the column oven temperature was 40 °C.

High-Throughput Equilibrium Solubility. Sample preparation for high-throughput equilibrium solubility determination is performed using a fully automated Hamilton liquid handling system. Starting from 10 mM DMSO stock solution, 20 μL of each sample is dispensed in triplicates in a polypropylene Corning 96-well plate. DMSO is evaporated in an evaporator (CombiDancer, Hettich) under vacuum and moderate heat of 40 °C for 40 min. Afterward 200 μL of buffer media is added (pH 6.8, chlorine-free phosphate buffer), and the plate is sealed and shaken overnight at 1000 rpm (TiMix5, Edmund Buehler) at an ambient temperature. After the phase separation of the supernatant and undissolved solid by 15 min centrifugation at 4000 rpm (2000 G), 100 μL of the supernatant is transferred into an intermediate 96-well plate. After the second centrifugation with the same conditions, an adequate volume of the supernatant is diluted 200 times into acetonitrile/water + internal standard (0.5 μM glyburide) by LC−HRMS analysis. Quantitation is done using a four-point external calibration curve from the DMSO stock solution (0.04, 0.2, 1.0, and 5.0 μM). The same analytical method as described in log D measurement was applied.

COMPUTATIONAL TECHNIQUES

MD Simulation Details. All MD simulations were performed using the GROMOS software package[55] and the GROMOS 54A7 force field[56] with the same setups as applied in ref 40, where simulations were carried out for CDPs **1**−**6**. There are two changes to the workflow in this study:

1 For CDPs **7**−**11**, the same seeding procedure as before was employed, that is, selecting a set of 100 seed conformers from enhanced sampling runs to perform parallel MD simulations of 100 ns length. When the subsequent CSMM is not converged, additional seed conformers were selected to be simulated. This process was repeated until the kinetic model was converged. As we often found that a single round of sampling was not sufficient, such an iterative procedure is time consuming. Therefore, for CDP **12** onward, we used the starting conformers of CDPs **1**, **3**, and **4** as an ensemble set of seeds. These seed conformers were adapted with in silico mutagenesis to a given peptide using an in-house script based on the MDAnalysis[57,58] package. The adapted seed conformers were equilibrated for 1 ns, followed by a 100 ns production run. Conformers that were too unfavorable were neglected. No additional rounds of resampling were performed for CDP **12** onward.

2 In general, each parallel simulation for a CDP is 100 ns. For CDPs **12**, **13**, **21**, and **22**, we prolonged the simulations to 200 ns to check the convergence of the kinetic models.

Markov State Modelling. For each trajectory, the sine and cosine of the backbone ϕ/ψ torsion angels were taken as the system descriptors, giving 40 feature dimensions. These were reduced into 9−12 collective coordinates (exact number depends on the peptide) by time-lagged independent component analysis (TICA).[59] No side chain information was included explicitly in the system description. The procedure was performed with PyEMMA.[60]

While a common nearest neighbor density-based algorithm[61] was used for the spatial clustering in ref 40, we employ in this study a hierarchical density-based clustering scheme developed by Sittel and Stock.[44] The Sittel−Stock algorithm was chosen because of two advantages: first, the previous scheme is memory inefficient and limits the total number of data points for clustering to about 100,000. This means that in each trajectory, only a relatively small number of frames could be clustered directly (i.e., a large stride was used), and the frames in between had to be mapped to the microstates in a cheap but inaccurate postprocessing step. The Sittel−Stock algorithm is memory-optimized, and thus, direct clustering of several million data points can be achieved without memory burden. Second and even more important, hierarchical clustering (i.e., clustering iteratively at different density thresholds) distinguishes better the metastable states residing at different free energy levels as shown by Weiß et al.[62]

The estimation of the transition matrix and the determination of the metastable states followed the same workflow as in ref 40. Bootstrapping was performed after the frames were clustered into microstates. For each bootstrap iteration, the transition matrix for the kinetic model was estimated by randomly picking n trajectories with replacement from the set of all trajectories, where n equals the total number of trajectories. Perron cluster cluster analysis (PCCA$^+$)[63] was performed to group microstates into metastable conformational states.

Analysis. *RMSD Calculation.* For selected CDPs, the backbone atom-positional RMSD of all trajectory frames with respect to the closed conformation was calculated using MDTraj.[64]

Hydrogen Bonding Patterns. For every CDP with threonine residues, the H-bond pattern from each frame of the simulations was extracted and the most abundant H-bond patterns involving any threonine side chain were stored. The difference in the H-bond patterns of different CDPs allows us to quantify how the location of threonine affects the formation of the closed conformation. This analysis was performed using MDTraj.[64]

ASSOCIATED CONTENT

Supporting Information

The Supporting Information is available free of charge at https://pubs.acs.org/doi/10.1021/acs.jmedchem.1c00775.

Hydrogen bonding patterns of CDPs **7**−**16**, comparison of PAMPA permeability log P_e versus the population of the closed conformation in water, correlation between clog P and log D decadiene/water, and correlation between clog P and log D octanol/water, implied time scales and CSMMs for each peptide, and metastable states projected onto the first two TICA dimensions for the first 6 decapeptides in chloroform and the 24 decapeptides in water (PDF)

SMILES strings of the 24 peptides (CSV)

https://doi.org/10.1021/acs.jmedchem.1c00775
J. Med. Chem. 2021, 64, 12761−12773

AUTHOR INFORMATION

Corresponding Author

Sereina Riniker − *Laboratory of Physical Chemistry, ETH Zürich, 8093 Zürich, Switzerland;* orcid.org/0000-0003-1893-4031; Email: sriniker@ethz.ch

Authors

Shuzhe Wang − *Laboratory of Physical Chemistry, ETH Zürich, 8093 Zürich, Switzerland;* orcid.org/0000-0001-7543-7387

Gerhard König − *Laboratory of Physical Chemistry, ETH Zürich, 8093 Zürich, Switzerland;* orcid.org/0000-0003-4898-2958

Hans-Jörg Roth − *Novartis Institutes for BioMedical Research, Novartis Pharma AG, 4056 Basel, Switzerland*

Marianne Fouché − *Novartis Institutes for BioMedical Research, Novartis Pharma AG, 4056 Basel, Switzerland*

Stephane Rodde − *Novartis Institutes for BioMedical Research, Novartis Pharma AG, 4056 Basel, Switzerland;* orcid.org/0000-0001-6559-2420

Complete contact information is available at: https://pubs.acs.org/10.1021/acs.jmedchem.1c00775

Notes

The authors declare no competing financial interest.

ACKNOWLEDGMENTS

The authors thank Jagna Witek, Gregor Weiss, and Benjamin Ries for helpful discussions. S.R. gratefully acknowledges financial support by the Swiss National Science Foundation (grant numbers 200021-178762).

ABBREVIATIONS

bRo5, beyond rule-of-five; CDP, cyclic decapeptide; CSMM, core-set Markov model; H-bonds, hydrogen bonds; PPI, protein−protein interaction; SASA, solvent-accessible surface area; TICA, time-lagged independent component analysis

REFERENCES

(1) Lipinski, C. A.; Lombardo, F.; Dominy, B. W.; Feeney, P. J. Experimental and Computational Approaches to Estimate Solubility and Permeability in Drug Discovery and Development Settings. *Adv. Drug Deliv. Rev.* **1997**, *23*, 3−25.

(2) Hopkins, A. L.; Groom, C. R. The Druggable Genome. *Nat. Rev. Drug Discov.* **2002**, *1*, 727−730.

(3) Overington, J. P.; Al-Lazikani, B.; Hopkins, A. L. How Many Drug Targets Are There? *Nat. Rev. Drug Discov.* **2006**, *5*, 993−996.

(4) Doak, B. C.; Over, B.; Giordanetto, F.; Kihlberg, J. Oral Druggable Space beyond the Rule of 5: Insights from Drugs and Clinical Candidates. *Chem. Biol.* **2014**, *21*, 1115−1142.

(5) Caron, G.; Kihlberg, J.; Goetz, G.; Ratkova, E.; Poongavanam, V.; Ermondi, G. Steering New Drug Discovery Campaigns: Permeability, Solubility, and Physicochemical Properties in the bRo5 Chemical Space. *ACS Med. Chem. Lett.* **2021**, *12*, 13−23.

(6) Villar, E. A.; Beglov, D.; Chennamadhavuni, S.; Porco, J. A.; Kozakov, D.; Vajda, S.; Whitty, A. How Proteins Bind Macrocycles. *Nat. Chem. Biol.* **2014**, *10*, 723−731.

(7) Tsomaia, N. Peptide Therapeutics: Targeting the Undruggable Space. *Eur. J. Med. Chem.* **2015**, *94*, 459−470.

(8) Naylor, M. R.; Bockus, A. T.; Blanco, M.-J.; Lokey, R. S. Cyclic Peptide Natural Products Chart the Frontier of Oral Bioavailability in the Pursuit of Undruggable Targets. *Curr. Opin. Chem. Biol.* **2017**, *38*, 141−147.

(9) Damjanovic, J.; Miao, J.; Huang, H.; Lin, Y.-S. Elucidating Solution Structures of Cyclic Peptides Using Molecular Dynamics Simulations. *Chem. Rev.* **2021**, *121*, 2292−2324.

(10) Adessi, C.; Soto, C. Converting a Peptide into a Drug: Strategies to Improve Stability and Bioavailability. *Curr. Med. Chem.* **2002**, *9*, 963−978.

(11) Zorzi, A.; Deyle, K.; Heinis, C. Cyclic Peptide Therapeutics: Past, Present and Future. *Curr. Opin. Chem. Biol.* **2017**, *38*, 24−29.

(12) Morrison, C. Constrained Peptides' Time to Shine? *Nat. Rev. Drug Discov.* **2018**, *17*, 531−533.

(13) Dougherty, P. G.; Sahni, A.; Pei, D. Understanding Cell Penetration of Cyclic Peptides. *Chem. Rev.* **2019**, *119*, 10241−10287.

(14) Rezai, T.; Bock, J. E.; Zhou, M. V.; Kalyanaraman, C.; Lokey, R. S.; Jacobson, M. P. Conformational Flexibility, Internal Hydrogen Bonding, and Passive Membrane Permeability: Successful in Silico Prediction of the Relative Permeabilities of Cyclic Peptides. *J. Am. Chem. Soc.* **2006**, *128*, 14073−14080.

(15) Rezai, T.; Yu, B.; Millhauser, G. L.; Jacobson, M. P.; Lokey, R. S. Testing the Conformational Hypothesis of Passive Membrane Permeability Using Synthetic Cyclic Peptide Diastereomers. *J. Am. Chem. Soc.* **2006**, *128*, 2510−2511.

(16) Whitty, A.; Zhong, M.; Viarengo, L.; Beglov, D.; Hall, D. R.; Vajda, S. Quantifying the Chameleonic Properties of Macrocycles and Other High-molecular-weight Drugs. *Drug Discov. Today* **2016**, *21*, 712−717.

(17) Matsson, P.; Kihlberg, J. How Big Is Too Big for Cell Permeability? *J. Med. Chem.* **2017**, *60*, 1662−1664.

(18) Yunger, L. M.; Cramer, R. D. Measurement and Correlation of Partition Coefficients of Polar Amino Acids. *Mol. Pharmacol.* **1981**, *20*, 602−608.

(19) König, G.; Boresch, S. Hydration Free Energies of Amino Acids: Why Side Chain Analog Data are not Enough. *J. Phys. Chem. B* **2009**, *113*, 8967−8974.

(20) Riniker, S. Toward the Elucidation of the Mechanism for Passive Membrane Permeability of Cyclic Peptides. *Future Med. Chem.* **2019**, *11*, 637−639.

(21) Alex, A.; Millan, D. S.; Perez, M.; Wakenhut, F.; Whitlock, G. A. Intramolecular hydrogen bonding to improve membrane permeability and absorption in beyond rule of five chemical space. *Med. Chem. Commun.* **2011**, *2*, 669−674.

(22) Naylor, M. R.; Ly, A. M.; Handford, M. J.; Ramos, D. P.; Pye, C. R.; Furukawa, A.; Klein, V. G.; Noland, R. P.; Edmondson, Q.; Turmon, A. C.; Hewitt, W. M.; Schwochert, J.; Townsend, C. E.; Kelly, C. N.; Blanco, M.-J.; Lokey, R. S. Lipophilic Permeability Efficiency Reconciles the Opposing Roles of Lipophilicity in Membrane Permeability and Aqueous Solubility. *J. Med. Chem.* **2018**, *61*, 11169−11182.

(23) Rossi Sebastiano, M.; Doak, B. C.; Backlund, M.; Poongavanam, V.; Over, B.; Ermondi, G.; Caron, G.; Matsson, P.; Kihlberg, J. Impact of Dynamically Exposed Polarity on Permeability and Solubility of Chameleonic Drugs Beyond the Rule of 5. *J. Med. Chem.* **2018**, *61*, 4189−4202.

(24) Le Roux, A.; Blaise, É.; Boudreault, P.-L.; Comeau, C.; Doucet, A.; Giarrusso, M.; Collin, M.-P.; Neubauer, T.; Kölling, F.; Göller, A. H.; Seep, L.; Tshitenge, D. T.; Wittwer, M.; Kullmann, M.; Hillisch, A.; Mittendorf, J.; Marsault, E. Structure−Permeability Relationship of Semipeptidic Macrocycles—Understanding and Optimizing Passive Permeability and Efflux Ratio. *J. Med. Chem.* **2020**, *63*, 6774−6783.

(25) Poongavanam, V.; Atilaw, Y.; Ye, S.; Wieske, L. H. E.; Erdelyi, M.; Ermondi, G.; Caron, G.; Kihlberg, J. Predicting the Permeability of Macrocycles from Conformational Sampling−Limitations of Molecular Flexibility. *J. Pharm. Sci.* **2021**, *110*, 301−313.

(26) Kamenik, A. S.; Kraml, J.; Hofer, F.; Waibl, F.; Quoika, P. K.; Kahler, U.; Schauperl, M.; Liedl, K. R. Macrocycle Cell Permeability Measured by Solvation Free Energies in Polar and Apolar Environments. *J. Chem. Inf. Model.* **2020**, *60*, 3508−3517.

(27) Ono, S.; Naylor, M. R.; Townsend, C. E.; Okumura, C.; Okada, O.; Lokey, R. S. Conformation and Permeability: Cyclic Hexapeptide Diastereomers. *J. Chem. Inf. Model.* **2019**, *59*, 2952−2963.
(28) Cipcigan, F.; Smith, P.; Crain, J.; Hogner, A.; De Maria, L.; Llinas, A.; Ratkova, E. Membrane Permeability in Cyclic Peptides is Modulated by Core Conformations. *J. Chem. Inf. Model.* **2021**, *61*, 263−269.
(29) Comeau, C.; Ries, B.; Stadelmann, T.; Tremblay, J.; Poulet, S.; Fröhlich, U.; Côté, J.; Boudreault, P.-L.; Derbali, R. M.; Sarret, P.; Grandbois, M.; Leclair, G.; Riniker, S.; Marsault, É. Modulation of the Passive Permeability of Semipeptidic Macrocycles: N-and C-Methylations Fine-Tune Conformation and Properties. *J. Med. Chem.* **2021**, *64*, 5365.
(30) Hoang, H. N.; Hill, T. A.; Fairlie, D. P. Connecting Hydrophobic Surfaces in Cyclic Peptides Increases Membrane Permeability. *Angew. Chem.* **2021**, *133*, 8466−8471.
(31) Danelius, E.; Poongavanam, V.; Peintner, S.; Wieske, L. H. E.; Erdélyi, M.; Kihlberg, J. Solution Conformations Explain the Chameleonic Behaviour of Macrocyclic Drugs. *Chem. Eur. J.* **2020**, *26*, 5231−5244.
(32) Wang, C. K.; Northfield, S. E.; Swedberg, J. E.; Colless, B.; Chaousis, S.; Price, D. A.; Liras, S.; Craik, D. J. Exploring Experimental and Computational Markers of Cyclic Peptides: Charting Islands of Permeability. *Eur. J. Med. Chem.* **2015**, *97*, 202−213.
(33) Furukawa, A.; Schwochert, J.; Pye, C. R.; Asano, D.; Edmondson, Q. D.; Turmon, A. C.; Klein, V. G.; Ono, S.; Okada, O.; Lokey, R. S. Drug-Like Properties in Macrocycles above MW 1000: Backbone Rigidity versus Side-Chain Lipophilicity. *Angew. Chem.* **2020**, *132*, 21755−21761.
(34) Nakajima, N.; Nakamura, H.; Kidera, A. Multicanonical Ensemble Generated by Molecular Dynamics Simulation for Enhanced Conformational Sampling of Peptides. *J. Phys. Chem. B* **1997**, *101*, 817−824.
(35) Buchete, N.-V.; Hummer, G. Coarse Master Equations for Peptide Folding Dynamics? *J. Phys. Chem. B* **2008**, *112*, 6057−6069.
(36) Vanden-Eijnden, E.; Venturoli, M.; Ciccotti, G.; Elber, R. On the Assumptions Underlying Milestoning. *J. Chem. Phys.* **2008**, *129*, 174102.
(37) Schütte, C.; Noé, F.; Lu, J.; Sarich, M.; Vanden-Eijnden, E. Markov State Models Based on Milestoning. *J. Chem. Phys.* **2011**, *134*, 204105.
(38) Witek, J.; Keller, B. G.; Blatter, M.; Meissner, A.; Wagner, T.; Riniker, S. Kinetic Models of Cyclosporin A in Polar and Apolar Environments Reveal Multiple Congruent Conformational States. *J. Chem. Inf. Model.* **2016**, *56*, 1547−1562.
(39) Witek, J.; Mühlbauer, M.; Keller, B. G.; Blatter, M.; Meissner, A.; Wagner, T.; Riniker, S. Interconversion Rates Between Conformational States as Rationale for the Membrane Permeability of Cyclosporines. *ChemPhysChem* **2017**, *18*, 3309−3314.
(40) Witek, J.; Wang, S.; Schroeder, B.; Lingwood, R.; Dounas, A.; Roth, H.-J.; Fouché, M.; Blatter, M.; Lemke, O.; Keller, B.; Riniker, S. Rationalization of the Membrane Permeability Differences in a Series of Analogue Cyclic Decapeptides. *J. Chem. Inf. Model.* **2018**, *59*, 294−308.
(41) Stadelmann, T.; Subramanian, G.; Menon, S.; Townsend, C. E.; Lokey, R. S.; Ebert, M.-O.; Riniker, S. Connecting the Conformational Behavior of Cyclic Octadepsipeptides with Their Ionophoric Property and Membrane Permeability. *Org. Biomol. Chem.* **2020**, *18*, 7110−7126.
(42) Fouché, M.; Schäfer, M.; Blatter, M.; Berghausen, J.; Desrayaud, S.; Roth, H.-J. Pharmacokinetic Studies around the Mono-and Difunctionalization of a Bioavailable Cyclic Decapeptide Scaffold. *ChemMedChem* **2016**, *11*, 1060−1068.
(43) Fouché, M.; Schäfer, M.; Berghausen, J.; Desrayaud, S.; Blatter, M.; Piéchon, P.; Dix, I.; Martin Garcia, A.; Roth, H.-J. Design and Development of a Cyclic Decapeptide Scaffold with Suitable Properties for Bioavailability and Oral Exposure. *ChemMedChem* **2016**, *11*, 1048−1059.
(44) Sittel, F.; Stock, G. Robust Density-based Clustering to Identify Metastable Conformational States of Proteins. *J. Chem. Theor. Comput.* **2016**, *12*, 2426−2435.
(45) Leo, A. J. Calculating log P_{oct} from Structures. *Chem. Rev.* **1993**, *93*, 1281−1306.
(46) Walter, A.; Gutknecht, J. Permeability of Small Nonelectrolytes Through Lipid Bilayer Membranes. *J. Membr. Biol.* **1986**, *90*, 207−217.
(47) Kubinyi, H. Lipophilicity and Biological Activity. *Arzneimittelforschung* **1979**, *29*, 1067−1080.
(48) Kubinyi, H. *Progress in Drug Research/Fortschritte der Arzneimittelforschung/Progrès des Recherches Pharmaceutiques*; Jucker, E., Ed.; Birkhäuser Basel: Basel, 1979; pp 97−198.
(49) Camenisch, G.; Folkers, G.; van de Waterbeemd, H. Review on Theoretical Passive Drug Absorption Models: Historical Background, Recent Developments and Limitations. *Pharm. Acta Helv.* **1996**, *71*, 309−327.
(50) Hannesschlaeger, C.; Horner, A.; Pohl, P. Intrinsic Membrane Permeability to Small Molecules. *Chem. Rev.* **2019**, *119*, 5922−5953.
(51) Fujikawa, M.; Nakao, K.; Shimizu, R.; Akamatsu, M. QSAR Study on Permeability of Hydrophobic Compounds with Artificial Membranes. *Bioorg. Med. Chem.* **2007**, *15*, 3756−3767.
(52) Furukawa, A.; Townsend, C. E.; Schwochert, J.; Pye, C. R.; Bednarek, M. A.; Lokey, R. S. Passive Membrane Permeability in Cyclic Peptomer Scaffolds is Robust to Extensive Variation in Side Chain Functionality and Backbone Geometry. *J. Med. Chem.* **2016**, *59*, 9503−9512.
(53) Leung, S. S. F.; Mijalkovic, J.; Borrelli, K.; Jacobson, M. P. Testing Physical Models of Passive Membrane Permeation. *J. Chem. Inf. Model.* **2012**, *52*, 1621−1636.
(54) Kansy, M.; Senner, F.; Gubernator, K. Physico-chemical High Throughput Screening: Parallel Artificial Membrane Permeability Assay in the Description of Passive Absorption Processes. *J. Med. Chem.* **1998**, *41*, 1007−1010.
(55) Schmid, N.; Christ, C. D.; Christen, M.; Eichenberger, A. P.; van Gunsteren, W. F. Architecture, Implementation and Parallelisation of the GROMOS Software for Biomolecular Simulation. *Comput. Phys. Commun.* **2012**, *183*, 890−903.
(56) Schmid, N.; Eichenberger, A. P.; Choutko, A.; Riniker, S.; Winger, M.; Mark, A. E.; van Gunsteren, W. F. Definition and Testing of the GROMOS Force-field Versions 54A7 and 54B7. *Eur. Biophys. J.* **2011**, *40*, 843−856.
(57) Michaud-Agrawal, N.; Denning, E. J.; Woolf, T. B.; Beckstein, O. MDAnalysis: A Toolkit for the Analysis of Molecular Dynamics Simulations. *J. Comput. Chem.* **2011**, *32*, 2319−2327.
(58) Gowers, R. J.; Linke, M.; Barnoud, J.; Reddy, T. J. E.; Melo, M. N.; Seyler, S. L.; Domanski, J.; Dotson, D. L.; Buchoux, S.; Kenney, I. M.; Beckstein, O. MDAnalysis: A Python Package for the Rapid Analysis of Molecular Dynamics Simulations. *Proceedings of the 15th Python in Science Conference*, 2016; pp 98−105.
(59) Pérez-Hernández, G.; Paul, F.; Giorgino, T.; De Fabritiis, G.; Noé, F. Identification of Slow Molecular Order Parameters for Markov Model Construction. *J. Chem. Phys.* **2013**, *139*, 015102.
(60) Scherer, M. K.; Trendelkamp-Schroer, B.; Paul, F.; Pérez-Hernández, G.; Hoffmann, M.; Plattner, N.; Wehmeyer, C.; Prinz, J.-H.; Noé, F. PyEMMA 2: A Software Package for Estimation, Validation, and Analysis of Markov Models. *J. Chem. Theor. Comput.* **2015**, *11*, 5525−5542.
(61) Lemke, O.; Keller, B. G. Density-based Cluster Algorithms for the Identification of Core Sets. *J. Chem. Phys.* **2016**, *145*, 164104.
(62) Weiß, R. G.; Ries, B.; Wang, S.; Riniker, S. Volume-scaled Common Nearest Neighbor Clustering Algorithm with Free-energy Hierarchy. *J. Chem. Phys.* **2021**, *154*, 084106.
(63) Deuflhard, P.; Weber, M. Robust Perron Cluster Analysis in Conformation Dynamics. *Lin. Algebra Appl.* **2005**, *398*, 161−184.
(64) McGibbon, R. T.; Beauchamp, K. A.; Harrigan, M. P.; Klein, C.; Swails, J. M.; Hernández, C. X.; Schwantes, C. R.; Wang, L.-P.; Lane, T. J.; Pande, V. S. MDTraj: A Modern Open Library for the

https://doi.org/10.1021/acs.jmedchem.1c00775
J. Med. Chem. 2021, 64, 12761−12773

Analysis of Molecular Dynamics Trajectories. *Biophys. J.* **2015**, *109*, 1528−1532.

https://doi.org/10.1021/acs.jmedchem.1c00775
J. Med. Chem. 2021, 64, 12761−12773